Triangular Platinum and Nickel Clusters: The "Tinker-Toy" Construction of Chains with High Nuclearity

Dennis J. Underwood,† Roald Hoffmann,* Kazuyuki Tatsumi,‡ Akira Nakamura,‡ and Yasuhiro Yamamoto§

Contribution from the CSIRO Division of Applied Organic Chemistry, G.P.O. Box 4331, Melbourne, Victoria 3001, Australia, Department of Chemistry, Baker Laboratory, Cornell University, Ithaca, New York 14853, Department of Macromolecular Science, Faculty of Science, Osaka University, Toyonaka, Osaka 560, Japan, and The Institute of Physical and Chemical Research, Wako-shi, Saitama 351, Japan. *Received December 3, 1984*

Abstract: The triangular metal carbonyls formed from the Ni group transition metals are remarkable in their propensity to form high nuclearity clusters just by associating into chains. Such chains are typified by the compounds $[Pt_3(\mu_2\text{-}CO)_3(CO)_3]_n^{2-}$ (n = 2, 3, 4, 5, 6, 10). However, there is a characteristic structural difference between the "tinker-toy" construction of stacks using Ni rather than Pt; the Ni carbonyl chains have a screw axis along the main axis, whereas the Pt chains have a simple threefold axis. Reasons for stacking and the requirements of the 2- charge for all chain lengths as well as the structural differences between Ni and Pt chains are discussed in terms of the calculated electronic structure of the dimer. As well as a necessary electron count for oligomerization, there exist monomers which have specific valence electron counts. For 42 valence electrons and acceptor ligands as bridges (e.g., $Pt_3(CNR)_6$) an equilateral triangle of metals is expected. When an extra two electrons are added, calculations show that distortion to an isosceles triangle or to a larger equilateral triangle is favored. Differences in electron count of various monomers are related to the types of bridging and terminal ligands present. For instance for bridging phosphido, PR_2, trimers the 44-electron species should be the stable one. The reasons for further deformation in such 44-electron trimers are addressed. In addition to oligomers, intercalation complexes are also known. For Ni there is the series $[Ni_{12}(CO)_{21}H_{4-n}]^{n-}$ where n = 2, 3, 4 and for Pt there are the compounds $[Pt_3(\mu_2\text{-}CNR)_3(CNR)_3]_2Hg$ where R = 2,6-dimethylphenyl and $[Pt(\mu_2\text{-}CO)_3(PPh\text{-}i\text{-}Pr_2)_3]_2Hg_2$. The reasons for the stability of these compounds are discussed in terms of the electronic structure of the Pt dimers at large monomer-monomer separation. On the basis of the known monomers, intercalates, and oligomers the existence of long-chain polymers is postulated. For $^1[Pt_3(CO)_6]_\infty$ the calculated bond structure indicates that oxidation or reduction of the neutral chain should result in stabilization. In many ways it is similar to the tetracyanoplatinate chains discussed previously in the literature. Partially occupied bands may result in Peierls distortions leading to structures similar to those observed for the pentamer and presumably the decamer. The band structure of $^1[Pt_3(CO)_6Hg]_\infty$ shows a valence band with much greater dispersion than the other bands. Partial occupation of this band (by replacing Hg with Cu, Ag, or Au) will most likely result in a pairing distortion to give a semiconductor.

The attention paid to polyhedral, multinuclear metal clusters derives both from the aesthetically pleasing act of creating polyhedral clusters with increasingly higher nuclearity and also from the desire to use these clusters as models of crystalline metal surfaces. Many reactions catalyzed on metallic surfaces are also seen to occur on smaller metal complexes.[1]

The smallest multinuclear metal cluster which can be considered as a model (albeit a highly simplistic one) of a metal surface is a triangular, trinuclear cluster. This unit forms the basis of many polyhedral clusters, indeed three out of the five platonic solids can be built up from this simple unit, viz., tetrahedron, octahedron, and icosahedron.

Triangular units can be recognized in polyhedra having 4-12 vertices, and for each of these molecular examples are known.[2] Once the polyhedra (closo structures) have been enumerated, more open frameworks having the same number of vertices can be found (nido, arachno, and hypho structures). A beautiful example of the opening of a closed structure is given by Lewis, Johnson, and co-workers in their discussion of the raft-like $Os_6(CO)_{17}[P(OMe)_3]_4$.[3]

There are still further ways to construct high nuclearity clusters from the basic "tinker-toy", triangular building block. If the building block is flat, and the $M_3(\mu_2\text{-}L')_3(L)_3$ unit **1** is particularly suited for this, then it can be simply stacked in one dimension. Two layers if eclipsed lead to a trigonal prism and if staggered to an octahedron of metals. The extension to oligomers and to a one-dimensional polymer is obvious. And not only on paper. These are real systems. We have discussed elsewhere[4] the beautiful

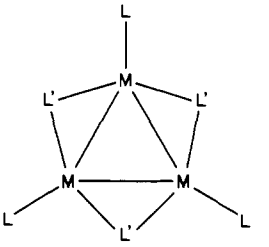

1

molybdenum chalcogenides of Chevrel, Sergent, and co-workers.[5] In the present contribution we trace the evolution to high nuclearity of the carbonyl clusters of the group 10 coinage metals, in particular platinum. For platinum the chains of triangular units are represented by the formula $[Pt(\mu_2\text{-}CO)_3(CO)_3]_n^{2-}$, where n = 2, 3, 4, 5, 6, 10.[6] The structures for n = 2 and 5 are shown in **2a**

† CSIRO Division of Applied Organic Chemistry.
* Cornell University.
‡ Osaka University.
§ The Institute of Physical and Chemical Research.

(1) For example, see: Muetterties, E. L.; Stein, J. *Chem. Rev.* **1979**, *79*, 479-490. Davis, S. C.; Klabunde, K. J. *Ibid.* **1982**, *82*, 153-208.
(2) See, for example: Cotton, F. A.; Wilkinson, G., "Advanced Inorganic Chemistry: A Comprehensive Text", 4th ed.; John Wiley and Sons: New York, 1980; Chapter 2.
(3) Goudsmit, R. J.; Johnson, B. F. G.; Lewis, J.; Raithby, P. R.; Whitmine, K. H. *J. Chem. Soc., Chem. Commun.* **1982**, 640-642.
(4) Hughbanks, T.; Hoffmann, R. *J. Am. Chem. Soc.* **1983**, *105*, 1150-1162.
(5) (a) Chevrel, R.; Sergent, M.; Prigent, J. *J. Solid State Chem.* **1971**, *3*, 515-519. (b) Potel, M.; Chevrel, R.; Sergent, M. *Acta Crystallogr., Sect. B* **1980**, *B36*, 1545-1548. (c) Potel, M.; Chevrel, R.; Sergent, M.; Armici, J. C.; Decroux, M.; Fischer, O. *J. Solid State Chem.* **1980**, *35*, 286-290. (d) Fischer, O. *Appl. Phys.* **1978**, *16*, 1-28. (e) Chevrel, R. In "Superconductor Materials Science: Metallurgy, Fabrication and Applications"; Foner, S., Schwartz, B. B., Eds.; Plenum Press: New York, 1981; Chapter 10.

0002-7863/85/1507-5968$01.50/0

and **2b**, respectively. Ideally the members of this series conform to a D_{3h} stacking arrangement. However, the crystal structures show a significant departure from ideality. The distortion in **2a** can be described as a lateral slip of one triangle relative to the

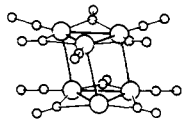

$(Pt_3(CO)_6)_2^{2-}$

2a

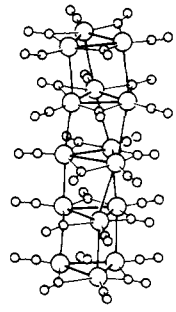

$(Pt_3(CO)_6)_5^{2-}$

2b

○ Pt

○ C,O

other, a slip in which the triangles are kept almost parallel. Higher members of the series show a more complex distortion; the trimer, $n = 3$, has a helical twist of about 13° from one unit to the next. The pentamer, **2b** ($n = 5$), is more complicated again since the angular distortion is mainly confined to the middle Pt_9 of the cluster. The distortion from top to bottom of the cluster is 64°.

To date the X-ray crystal structures of $n = 2$, 3, 4, and 5 have been elucidated.[6a] In all, the intratriangle Pt–Pt distance is 2.7 Å, typical of a single bond,[7] and the intertriangle Pt–Pt distance is about 3.0 Å, indicating that this interaction is somewhat less than that of a single bond.

The existence of the monomer $[Pt_3(CO)_6]^{2-}$ in solution has been inferred from ^{195}Pt NMR studies.[6c] Such a species, having 44 valence electrons, is quite rare. Another complex with this electron count is $Pt_3(\mu_2\text{-}PPh_2)_3Ph(PPh_3)_2$ which possesses an isosceles triangle of metals rather than one which is equilateral; two Pt–Pt distances are 2.79 Å, and the third is 3.63 Å.[8a] One metal–metal bond has been broken in this cluster. We will return to a discussion of its electronic structure below.

Platinum, however, shows a remarkable tendency to form neutral triangular clusters of the Pt_3L_6 type. Examples are $Pt_3(\mu_2\text{-}CNBu^t)_3(CNBu^t)_3$,[9a] $Pt_3(\mu_2\text{-}Ph)(\mu_2\text{-}PPh_2)(\mu_2\text{-}SO_2)(PPh_3)_3$,[9b] and $[Pt_3(\mu_2\text{-}PPh_2)_2(\mu_2\text{-}H)(PPh_3)_3]^+$[9c] amongst others.[9d] In each case the Pt_3 triangle is approximately equilateral, with the Pt–Pt distances being of the order of a single bond. The number of cluster electrons in each of these compounds is 42. Structure **3** shows the general framework for a specific example, the isocyanide complex.

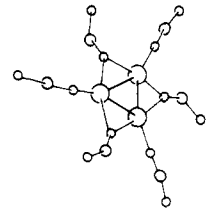

3

Another compound in this series, which, incidentally, is structurally related to the raft-like $Os_6(CO)_{17}[P(OMe)_3]_4$ cluster mentioned previously,[3] is $\{Pt_3(CO)_3[Fe(CO)_4]_3\}^q$ ($q = 1-, 2-$).[8b] The structure of this compound is shown in **4** and comparison with **3** emphasizes the special relationship between $Fe(CO)_4$ (C_{2v}) and CNR groups. X-ray diffraction studies indicate that the Pt_3

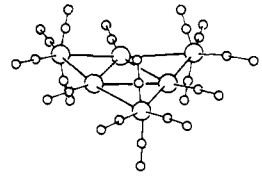

$\{Pt_3(CO)_3[Fe(CO)_4]_3\}^q$

4

triangle is equilateral with Pt–Pt distances 2.66 Å for $q = 1-$ and 2.75 Å for $q = 2-$, i.e., reduction causes a significant lengthening of the average Pt–Pt bond distance. More will be said of this later.

A question that arises from the above survey is the following: why does the majority of Pt_3 clusters conform to the 42-electron count? A related question is how are the monomeric $Pt_3(CO)_6$ units held together to form the higher nuclearity clusters? Will such a stacking scheme produce stable long-chain polymers and does the as yet uncharacterized polymer $[Pt(CO)_2]$[6a] have this structure?

The Pt_3L_6 unit itself can serve as a ligand. Thus we have $[Pt_3(CO)_3(PCy_3)_3]AuPCy_3^+$, a complex with an AuL^+ unit attached,[10b] and some fascinating complexes in which two Pt_3L_6 units surround a Hg or Hg_2 entity. The electronic structure of the latter complexes will be discussed in some detail further on in this paper.

Other members of the nickel group transition metals do not share Pt's tendency to form stacked triangular clusters. Ni for instance forms an octahedral $[Ni_3(\mu_2\text{-}CO)_3(CO)_3]_2^{2-}$ cluster **5**[6a,11a] and an octahedral-based $[Ni_3(\mu_2\text{-}CO)_3(CO)_3]_3^{2-}$ cluster.[11b] There is a higher nuclearity Ni cluster $[Ni_{12}(CO)_{21}]^{4-}$ as shown in **6**,[11c] but this is similar to the trimer mentioned previously.[11b] The connection between the trimer and **6** becomes clearer when one realizes the isolobal relationship shown in **7**.[12] To arrive at this series of analogies, bridging CO's are disconnected in a cyclic fashion and localized to one metal. The isolobal relationship

(6) (a) For a review of large metal clusters see: Chini, P. *J. Organomet. Chem.* **1980**, *200*, 37–61. (b) Calabrese, J. C.; Dahl, L. F.; Cavalieri, A.; Chini, P.; Longoni, G.; Martinengo, S. *J. Am. Chem. Soc.* **1974**, *96*, 2614–2616. (c) Longoni, G.; Chini, P. *Ibid.* **1976**, *98*, 7225–7231. (d) For a recent review of platinum carbonyls see: Clark, H. C.; Jain, V. K. *Coord. Chem. Rev.* **1984**, *55*, 151–204.

(7) Skapski, A. C.; Troughton, P. G. H. *J. Chem. Soc. A* **1969**, 2772–2781. Cheung, K. K.; Cross, R. J.; Forrest, K. P.; Wardle, R.; Mercer, M. *J. Chem. Soc., Chem. Commun.* **1971**, 875–876.

(8) (a) Taylor, N. J.; Chieh, P. C.; Carty, A. J. *J. Chem. Soc., Chem. Commun.* **1975**, 448–449. (b) Longoni, G.; Manassero, M.; Sansoni, M. *J. Am. Chem. Soc.* **1980**, *102*, 7973–7974.

(9) (a) Green, M.; Howard, J. A. K.; Murray, M.; Spencer, J. L.; Stone, F. G. A. *J. Chem. Soc., Dalton Trans.* **1977**, 1509–1514. (b) Evans, D. G.; Hughes, G. R.; Mingos, D. M. P.; Bassett, J.-M.; Welch, A. J. *J. Chem. Soc., Chem. Commun.* **1980**, 1255–1257. (c) Bellon, P. L.; Ceriotti, A.; Demartin, F.; Longoni, G.; Heaton, B. T. *J. Chem. Soc., Dalton Trans.* **1982**, 1671–1677. (d) Moody, D. C.; Ryan, R. R. *Inorg. Chem.* **1977**, *16*, 1052–1055. Scherer, O. J.; Konrad, R.; Guggolz, E.; Ziegler, M. L. *Angew. Chem. Suppl.* **1982**, 730–738. Albinati, A. *Inorg. Chim. Acta* **1977**, *22*, L31–L32.

(10) (a) Booth, G.; Chatt, J. *J. Chem. Soc. A* **1969**, 2131–2132. Booth, G.; Chatt, J.; Chini, P. *J. Chem. Soc., Chem. Commun.* **1965**, 639–640. (b) Briant, C. E.; Wardle, R. W. M.; Mingos, D. M. P. *J. Organomet. Chem.* **1984**, *267*, C49–C51.

(11) (a) Calabrese, J. C.; Dahl, L. F.; Cavalieri, A.; Chini, P.; Longoni, G.; Martinengo, S. *J. Am. Chem. Soc.* **1974**, *96*, 2616–2618. (b) Longoni, G.; Chini, P. *Inorg. Chem.* **1976**, *15*, 3029–3031. (c) Chini, P.; Longoni, G.; Manassero, M.; Sansoni, M. "Abstracts of the Eighth Meeting of the Italian Association of Crystallography"; Ferrara, 1977; Communication 34. (d) Borach, R. W.; Dahl, L. F.; Longoni, G.; Chini, P.; Schultz, A. J.; Williams, J. M. *Adv. Chem. Ser.* **1977**, *167*, 93–110. Ceriotti, A.; Chini, P.; Pergola, R. D.; Longoni, G. *Inorg. Chem.* **1983**, *22*, 1595–1598. (e) These compounds have been described as carbonyl clusters of a hexagonal close packed Ni fragment since the stacking of metals is aba.

(12) Elian, M.; Chen, M. M. L.; Mingos, D. M. P.; Hoffmann, R. *Inorg. Chem.* **1976**, *15*, 1148–1155. Albright, T. A.; Hofmann, P.; Hoffmann, R. *J. Am. Chem. Soc.* **1977**, *99*, 7546–7557. Pinhas, A. R.; Albright, T. A.; Hofmann, P.; Hoffmann, R. *Helv. Chim. Acta* **1980**, *63*, 29–49. Hoffmann, R. *Angew. Chem., Intl. Ed. Engl.* **1982**, *21*, 711–724.

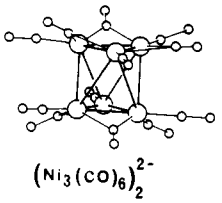

$(Ni_3(CO)_6)_2^{2-}$

5

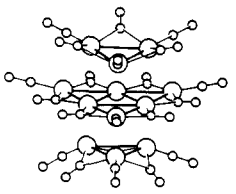

$(Ni_{12}(CO)_{21}H_{4-n})^{n-}$ n = 2,3,4.

6

between $d^{10}ML_2$ (C_{2v}) and d^8ML_4 (C_{2v}) also provides a rationale for the existence of the $Fe(CO)_4$-bridged cluster **4**. There is a

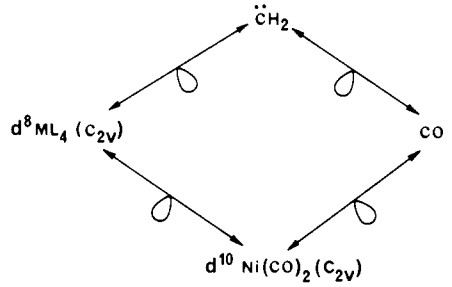

7

difference between the nickel trimer **6** ($n = 4$) and the platinum trimer; the former has two extra electrons which may be assigned to the sandwiched $Ni_3(CO)_9$ fragment. The reasons for this partitioning of electrons will be discussed later. The Ni_{12} cluster shows a readiness to form hydrides as indicated in **6**, $n = 2$ and 3. Neutron diffraction experiments have placed the hydrides in octahedral holes produced by the metal atoms.[11d,e] The importance of these derivatives of the Ni clusters will become clearer later when the intercalates of the Pt triangular compounds are discussed.

Even though many simple Pd_3 triangular clusters are known,[13a,b] there is only one cluster in which the stacking of these units can be seen, viz., $[Fe_6Pd_6(CO)_{24}H]^{3-}$, in which two Pd_3 units form an octahedron, with a complex arrangement of ligands including triply bridging $Fe(CO)_2$ fragments.[13c]

Among the Pd_3L_6 clusters there are some which have 44 cluster electrons, viz., $Pd_3X(PPh_2)_2(PR_3)_3^+$ where X = Cl, Br, or SCF_3 and R = Ph or Et.[13b] When X = Cl and R = Et, the Pd–Pd distance is on average 2.92 Å and the triangle is approximately equilateral. This distance should be contrasted with the Pd–Pd distance of 2.74 Å for the sum of metallic radii.[13c] Again, an excess of cluster electrons over 42 have resulted in a lengthening of the metal–metal distances.

The Monomer: M_3L_6

There are a number of literature studies on the electronic structure of triangular metal clusters.[14,15] These involve qualitative

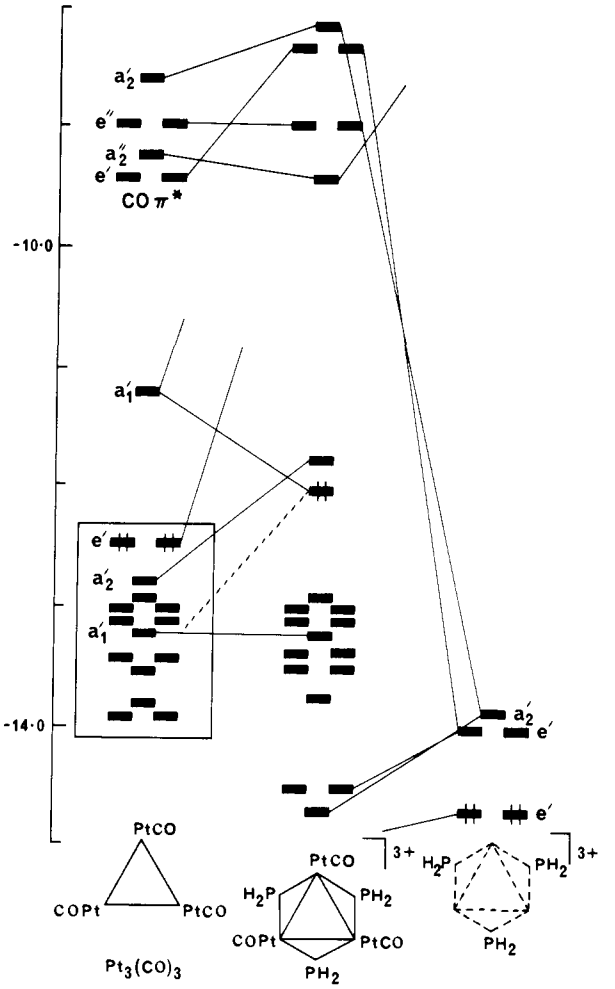

Figure 1. Partial fragment molecular orbital analysis of $Pt_3(\mu_2\text{-}CO)_3(CO)_3$ in which the metals and the terminal CO's are taken to be in one fragment and bridging CO's in the other.

symmetry analysis,[11a,b] extended Hückel,[14d-g,15] discrete variational X_α,[14h] Fenske–Hall,[14i] modified INDO,[14j,k] and chemical pseudopotential[14l,m] calculations. Of particular relevance to this work are the calculations on the monomers, Pt_3L_6,[14d,g,i,15] $Ni_3(\mu_2\text{-}CO)_3(CO)_3$,[14j] and the Ni and Pt dimers and trimers.[14k-m,15b]

As a starting point in our studies of the stacks of triangular clusters, we performed extended Hückel calculations on $Pt_3(\mu_2\text{-}CO)_3(CO)_3$ and $Pt_3(\mu_2\text{-}CNH)_3(CNH)_3$ (a model for the *tert*-butyl isocyanide cluster, **3**) and $Ni_3(\mu_2\text{-}CO)_3(CO)_3$ (see **8**). Details of the calculational method, the geometry, and the parameters used are given in the Appendix.

The results of these calculations confirm the observations of the previous workers; a summary, from a viewpoint similar to that used by Mealli[15a] for $Pt_3(\mu_2\text{-}CO)_3(CO)_3$, follows.

(13) (a) For example: Bushnell, G. W.; Dixon, K. R.; Moroney, P. M.; Rattray, A. D.; Wan, C. *J. Chem. Soc., Chem. Commun.* **1977**, 709–710 and references therein. (b) Cartwright, S. J.; Dixon, K. R.; Rattray, A. D. *Inorg. Chem.* **1980**, *19*, 1120–1124 and references therein. (c) Longoni, G.; Manassero, M.; Sansoni, M. *J. Am. Chem. Soc.* **1980**, *102*, 3242–3244.

(14) (a) Cotton, F. A.; Haas, T. E. *Inorg. Chem.* **1964**, *3*, 10–17. (b) Wei, C. H.; Dahl, L. F. *J. Am. Chem. Soc.* **1968**, *90*, 3960–3969. (c) Ruff, J. K.; White, R. P., Jr.; Dahl, L. F. *Ibid.* **1971**, *93*, 2159–2176. (d) Lauher, J. W. *Ibid.* **1978**, *100*, 5305–5315. (e) Dedieu, A.; Hoffmann, R. *Ibid.* **1978**, *100*, 2074–2079. (f) Schilling, B. E. R.; Hoffmann, R. *Ibid.* **1979**, *101*, 3456–3467. (g) See ref 9b and the following: Evans, D. G.; Mingos, D. M. P. *Organometallics* **1983**, *2*, 435–447. (h) Delley, B.; Manning, M. C.; Ellis, D. E.; Berkowitz, J.; Trogler, W. C. *Inorg. Chem.* **1982**, *21*, 2247–2253. (i) Rives, A. B.; Xiao-Zeng, Y.; Fenske, R. F. *Ibid.* **1982**, *21*, 2286–2294. (j) Pacchioni, G.; Fantucci, D.; Valenti, V. *J. Organomet. Chem.* **1982**, *224*, 89–105. (k) Fantucci, P.; Pacchioni, G.; Valenti, V. *Inorg. Chem.* **1984**, *23*, 247–253. (l) Chang, K. W.; Wooley, R. G. *J. Phys. C: Solid State Phys.* **1979**, *12*, 2745–2767. (m) Bullett, D. W. *Chem. Phys. Lett.* **1985**, *115*, 450–453.

(15) (a) Mealli, C. *J. Am. Chem. Soc.*, in press. (b) McEvoy, N. A., Part II Thesis, University of Oxford, 1980. McEvoy, N. A.; Evans, D. G.; Mingos, D. M. P., unpublished results.

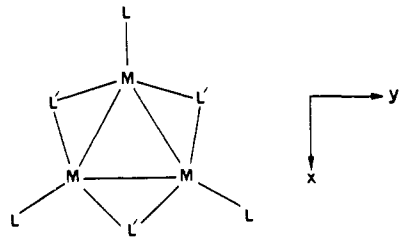

8

(a) M = Pt, L = L' = CO

(b) M = Pt, L = L' = CNH

(c) M = Pt, L = CO, L' = SO_2

(d) M = Pt, L = CO, L' = PH_2

Figure 1 shows the frontier molecular energy levels of **8a** together with those of the fragments $Pt_3(CO)_3$ (terminal ligands) and $(CO)_3$ (bridging ligands).

The HOMO of the 42 cluster electron monomer **8a** is an orbital of a_1' symmetry in which the wave function is localized mainly on the metals (77%) and lies in the plane of the triangle. This orbital is shown in **9**. It is clearly metal–metal bonding.

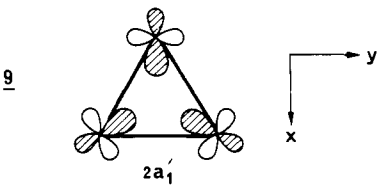

The LUMO is of a_2'' symmetry and is about 1.6 eV higher in energy. In this orbital most of the electron density is localized on the bridging CO ligands (63%). In a fragment interaction sense it is composed of (μ_2-CO) π^*, lying out of the plane of the metals, interacting in a bonding way with Pt p_z. This orbital is represented by **10**.

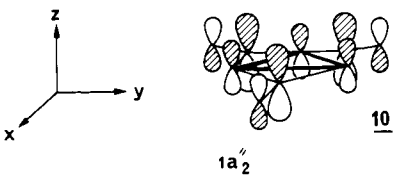

Close to this orbital (0.1 eV higher) is an orbital which again places most of its electron density on the bridging CO's (68%). This time it derives from the CO π^* orbitals which lie in the plane of the metal triangle. The symmetry of this orbital is a_2' and is shown in **11**. As **11** indicates, the interaction is Pt–CO bonding (σ) but Pt–Pt σ^*.

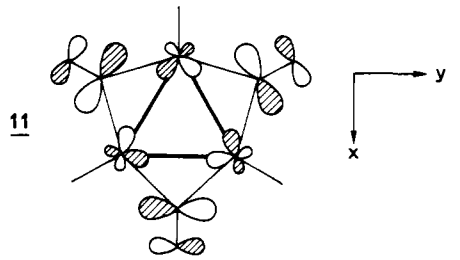

In addition to the interaction between the a_2' and a_2'' levels of the fragments, the e' and e'' sets accompanying these orbitals under D_{3h} symmetry also mix and set up bonding and antibonding combinations (Figure 1). In essence the interworking of all of these orbitals creates a group of mainly CO π^* (both bridging and terminal) levels just above the HOMO of the neutral cluster. It is these orbitals which are important in the reduced compounds.

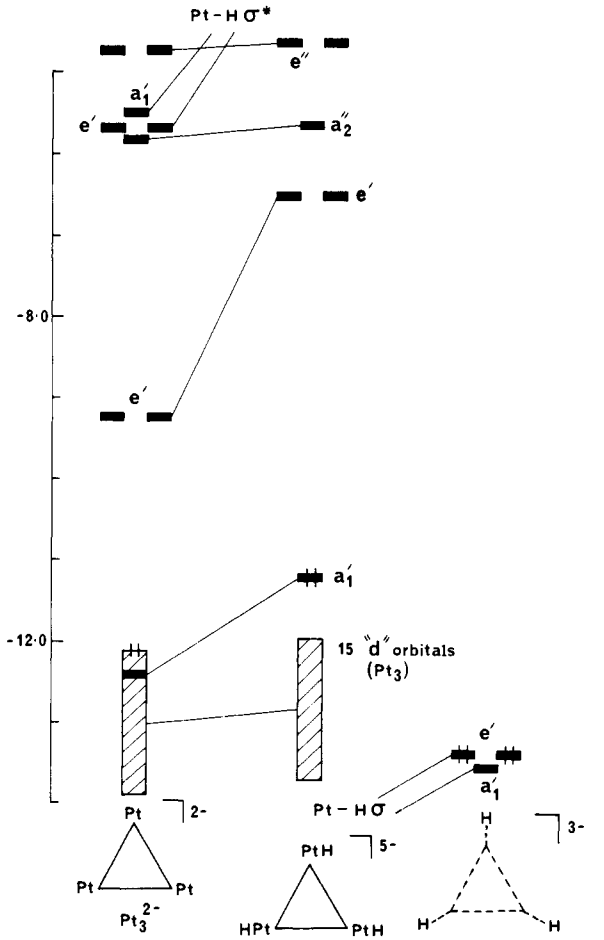

Figure 2. Fragment molecular orbital diagram showing the perturbation of Pt_3^{2-} orbitals by interaction with three H^- atoms of the appropriate symmetry.

It was mentioned in the introduction to this paper that the favored valence electron count for these triangular Ni group clusters is 42 with the reduced 44-electron clusters being rare. Application of the polyhedral skeletal electron pair approach[17] leads us to the same conclusions. For transition-metal carbonyl-ring compounds there should be $16n$ valence electrons where n is the number of vertices of the ring. As a result, compounds such as $Os_3(CO)_{12}$ with 48 valence electrons are predicted to have an equilateral triangle of metals.[17] Replacement of the $Os(CO_4)$ (C_{2v}) fragment with $Pt(CO)_2$, its isolobal analogue, leads to a decrease in the valence electron count of 2 per metal fragment replaced. The valence electron count of $Pt_3(CO)_6$ is then predicted to be 42. One would then expect changes in structure when these clusters are reduced or oxidized.

Before describing, in some detail, the electronic reasons for the architectural changes observed in the reduced M_3L_6 compounds, it is important to examine the changes in the molecular orbitals of the 42 valence electron compounds as occasioned by the electronic demands of various ligands.

Terminal Ligands

In general there are two types of terminal ligands observed for these clusters. The first are those which function as primarily

(16) It is of interest to note that in qualitatively formulating an interaction diagram such as this from known fragment orbitals (for example see ref 14f) one is tempted to unbridge the CO's and interact three $Pt(CO)_2$ (C_{2v}) units. For this case ^{13}C NMR suggests that there is no interchange of bridging and terminal ligands even at 60 °C.[9a,24] This observation has been confirmed by Mealli, who has found that the potential energy for the conversion of the bridged D_{3h} to the all terminal D_{3h} structure minimizes at the former.[15a]

(17) For a recent paper on this approach see ref 14g and the following: Mingos, D. M. P. *J. Chem. Soc., Chem. Commun.* **1983**, 706–708. Mingos, D. M. P.; Evans, D. G. *J. Organomet. Chem.* **1983**, *251*, C13–C16. Mingos, D. M. P. *Acc. Chem. Res.* **1984**, *17*, 311–319.

σ donors. This group is typified by the ligand PR_3. Second, there are those which in addition to their σ donor capabilities also have the facility of being π^* acceptors and perhaps π donors. CO and CNR fall into this category. The third group contains ligands which primarily have a π-donor ability, such as the halogens. As yet simple trigonal clusters having terminal ligands from this last group have not been prepared.

The bridging ligands have both σ- and π-bonding propensities and can be divided into those with degenerate perpendicular π orbitals, such as CO and CNR, and those which have only one orbital of π symmetry, namely SO_2 and PR_2. More will be said about the bridging ligands later. First let us consider the terminal ligands.

Although we have already described the MO picture for the entire complex (Figure 1), it is instructive to begin our discussion from a naked equilateral triangle of metals and follow the molecular orbitals as they are perturbed by the addition of groups of ligands. This approach is detailed in Figures 2 and 3.

Figure 2 is the molecular orbital diagram showing perturbation of the Pt_3^{2-} fragment orbitals by interaction with three H^- ions to produce three Pt–H σ bonds. The electron-counting scheme chosen was to produce a full Pt_3 d block in the composite complex. Since the a_1' orbital, composed of mainly Pt s orbitals, is stabilized and resides among the d orbitals, an extra 2 electrons were added to produce $Pt_3H_3^{5-}$, a compound with a large HOMO–LUMO gap.

The three hydrides transform as $a_1' + e'$. There are orbitals of appropriate symmetry in the Pt 5d block, but these orbitals are at low energy and contracted; the primary interaction is with Pt 6s and 6p. From these valence orbitals one can form two $a_1' + e'$ sets. A typical three-orbital pattern results—the metal–H σ combinations to low energy, the obligatory σ^* counterpart moving high up, and one $a_1' + e'$ set in the middle, forming the HOMO and LUMO of the $Pt_3H_3^{5-}$ complex.

What happens when the terminal ligands have π-type symmetry orbitals in addition to these of local σ symmetry? To pursue this, the terminal hydrides were replaced with CO's at the appropriate distances. In general, the σ interactions between the metals and the CO ligands are the same as those for the hydrides except that for the former the interaction is stronger. This is because of the directionality of the CO lone pairs.

Figure 3 shows the result of "turning on the π interactions". The main feature of this interworking of orbitals is the appearance of the six mainly CO π^* orbitals, which remain unfilled and lie just above the HOMO (for the $[Pt_3(CO)_3]^{2-}$ complex). The unoccupied orbitals of the Pt_3^{2-} fragment, unperturbed by σ interaction with the terminal ligands, are now pushed to higher energy by the CO π and π^* orbitals.

The stabilizing effect of the π interactions between the CO ligands and the Pt_3 nucleus can be appreciated by comparing the energy for this interaction with that for the hydrides. For $Pt_3H_3^{5-}$ the stabilization energy, defined as the difference between the total one-electron energies of the formed complex and the sum of the total energies for the individual fragments, is −4.68 eV. For $Pt_3(CO)_3^{2-}$ this value is −10.41 eV; the increased stabilization is due to better σ bonding and the effects of the π^* orbitals. A further comparison can be made with a member from another group of ligands, a π donor such as Cl^-. In this case the stabilization energy for $Pt_3Cl_3^{5-}$ from its fragments is only −1.32 eV. The relevant Cl_3^{3-} orbitals, the σ type $a_1' + e'$ and the π types $a_2' + e'$ and $a_2'' + e''$, are all at around −15.0 eV, close to the bottom of the Pt_3 d band. As a result, repulsive interaction between filled orbitals predominates and the stabilization energy is reduced. Unlike $(CO)_3$ there are no unoccupied π^* levels to enforce a favorable displacement of energy levels.

Thus, in general, for the Pt_3L_3 fragment, terminal π donors such as Cl^- are less stabilizing than H^- whereas π acceptors such as CO are more stabilizing.

Bridging Ligands

All of the bridging ligands have local π-symmetry orbitals available for bonding to the two metal atoms. In some cases there

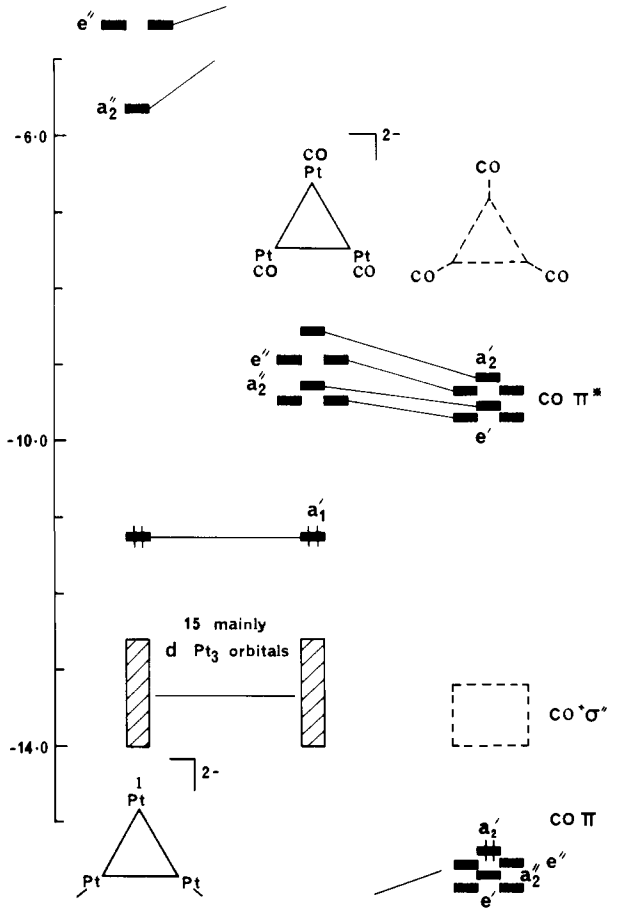

Figure 3. Interaction diagram between the already σ-bonded $Pt_3(CO)_3^{2-}$ and the π and π^* ligand orbitals. The CO "σ" orbital position is shown but interaction of these orbitals with the metal triangle has already been taken into account.

are two such orbitals; orthogonal π sets such as one finds for CO and CNR. In other cases there is but one π-symmetry orbital as with the nonbonding orbitals of the PR_2, SO_2, and the π system of $C_6H_5^-$. The D_{3h} symmetry adapted combinations of σ, π, and σ^* orbitals for the $(CO)_3$ fragment are shown in **12**.

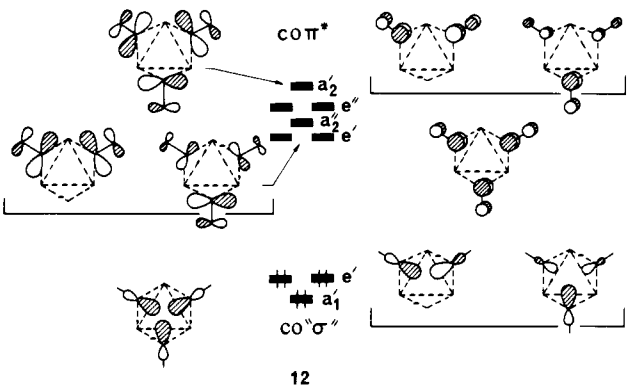

12

To discover the effect of different types of bridging ligands, calculations were performed on the model compounds $Pt_3(\mu_2\text{-}CNH)_3(CNH)_3$ (**8b**), $Pt_3(\mu_2\text{-}SO_2)_3(CO)_3$ (**8c**), and $[Pt_3(\mu_2\text{-}PH_2)_3(CO)_3]^{3+}$ (**8d**). There are some important similarities and equally significant differences between the bridging fragments, so it is important to see the relative energies of their valence orbitals. These are indicated in Figure 4. Each entity within the $(\mu_2\text{-L})_3$ fragment carries a lone pair and one or two acceptor orbitals. These valence orbitals are shown in **13**, but not on the same energy scale. To really compare these one must in fact look at the energies, and these are shown in Figure 4. One can see that PH_2 (taken in **13** as PH_2^+) is qualitatively different from CO

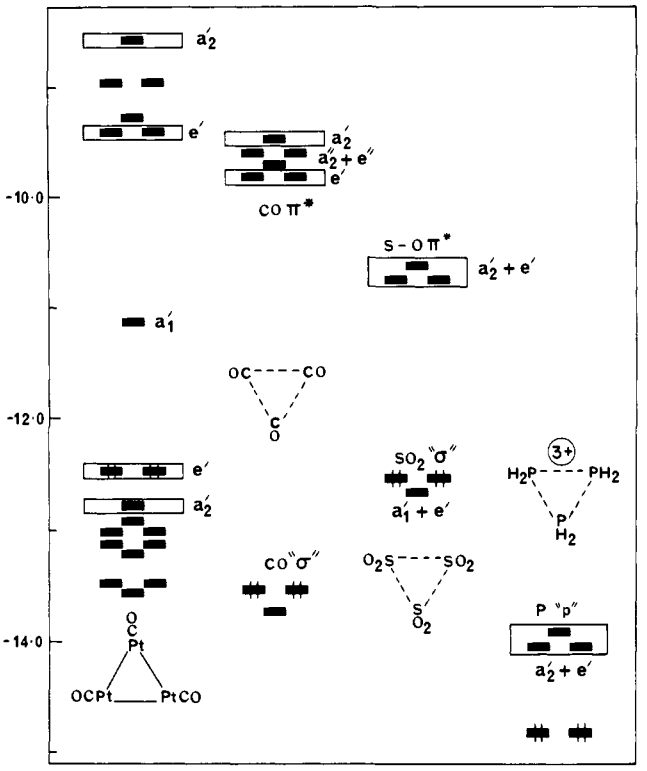

Figure 4. Comparison of the frontier orbitals of various bridging ligands with those of the $Pt_3(CO)_3$ fragment. Those orbitals which are boxed are relevant to the discussion.

and SO_2 in that the combinations of the p-type "acceptor" orbitals of PH_2^+ are way down in energy, below the $Pt_3(CO)_3$ d block. No wonder that no one thinks of PH_2^+. A better starting point would be PH_2^-, with these p-type orbitals filled. But then the analogy to CO and SO_2 would be obscured.

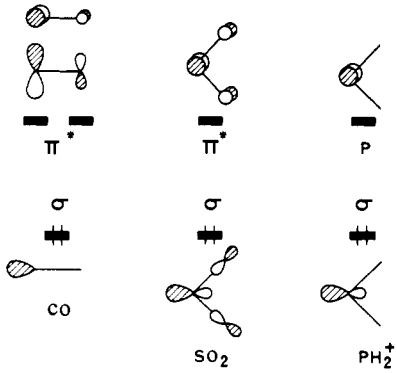

13

Let us in fact construct an interaction diagram for the phosphido-bridged trimer, to see what differences ensue from the energetic disparity in these orbital energies. This is done in Figure 5. Please compare this interaction diagram to that of $Pt_3(CO)_3$ and $(CO)_3$ (Figure 1). In both cases ligand donor orbitals are stabilized and there is a Pt-dominated a_1' orbital just above the d block. In the μ_2-CO case the symmetry combination of the π^* orbitals of CO is important, but it remains empty. In μ_2-PH_2 the analogous p orbitals (see **13** and Figure 4) are very low in energy, just below the d block. They find orbitals of appropriate energy with which to interact and must be filled.

But now we must watch our electron counting and consider the consequences of transferring electrons to PH_2^+ making it PH_2^-. In $Pt_3(CO)_3$ we have a d^{10} Pt(0) configuration, and a total of 36 valence electrons, counting the 3 CO lone pairs. In $Pt_3(CO)_6$ we have 42 electrons, and Pt is still Pt(0), d^{10}. Fifteen mainly d-type Pt orbitals are in the band at the bottom of Figure 1. In $Pt_3(CO)_3(PH_2)_3^{3+}$ we also have 42 electrons, as we expect from the aforementioned analogy between PH_2^+ and CO. But a better picture would be to view this complex as $[Pt_3(CO)_3]^{6+}[PH_2^-]_3^{3-}$, i.e., Pt(II) d^8. Note that there are 14 low-lying orbitals in Figure 5. Of these, 3 have their wave functions located mainly (60–80%) on the ligands and 11 are mainly (80–100%) Pt d in character. The 12th (to make three Pt(II) systems, 24 electrons) orbital is a_2'. It is clearly destabilized, an antibonding combination of PH_2 p orbitals and in-plane metal d orbitals. Explicitly, 75% of this orbital is Pt d, 2.5% Pt p, and 19% P. Its counterpart, the bonding combination, the lowest orbital in Figure 5, has a greater contribution from Pt p which overlaps in a bonding way with the P functions. In this case there is 8.5% Pt p and 11% Pt d, and the remainder of the wave function is split almost equally between the two types of ligands. These orbitals are shown in **14**. Figure 5 shows that a_2' is approximately the same energy as a Pt–Pt bonding a_1' orbital that comes down in energy. The 42-electron system can fill only one of these, and it would be expected to be unstable to a second-order Jahn–Teller deformation. The 44-electron cluster, on the other hand, would have a nice gap between filled and unfilled levels.

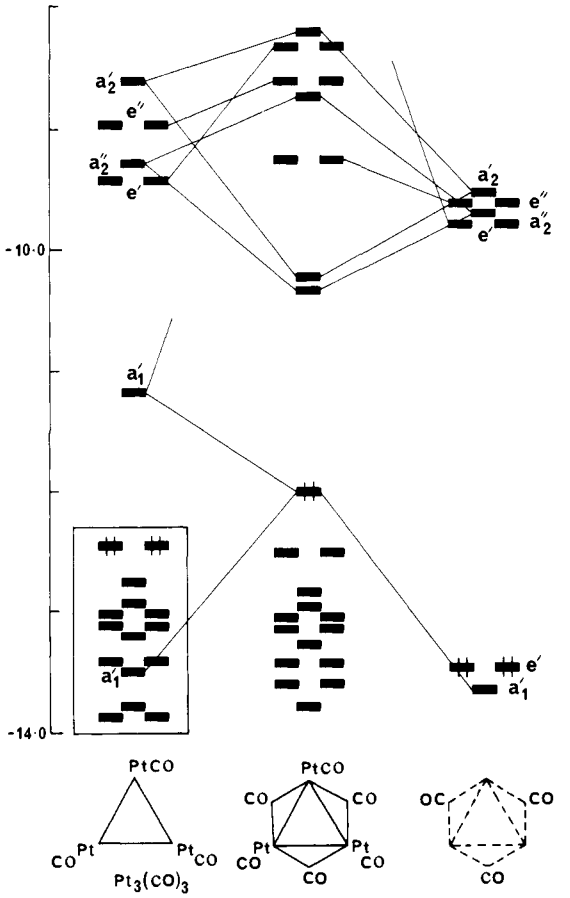

Figure 5. Interaction diagram for $Pt_3(\mu_2\text{-}PH_2)_3(CO)_3^{3+}$ in terms of the fragments $Pt_3(CO)_3$ and $(\mu_2\text{-}PH_2)_3$.

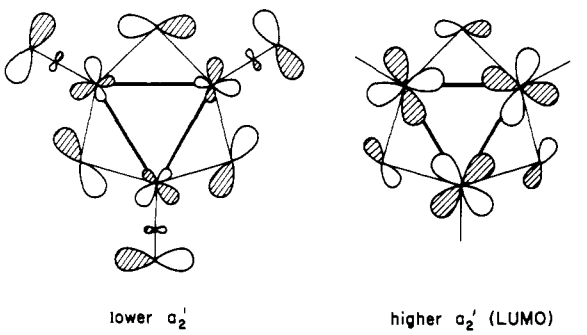

14

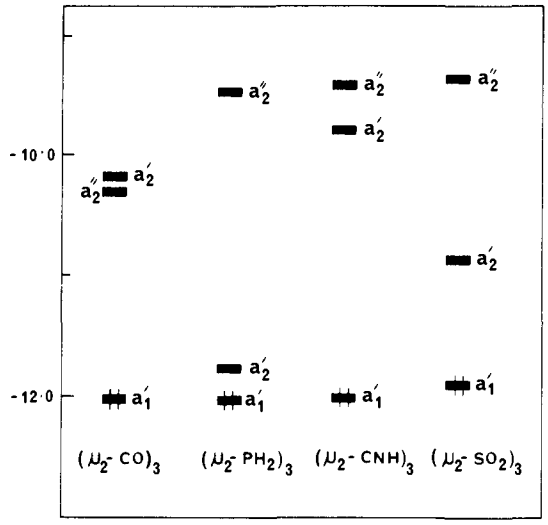

Figure 6. Valence orbitals of $Pt_3(\mu_2\text{-}L)_3(CO)_3$ complexes with L = CO, SO_2, PH_2, and CNH compared on an absolute energy scale.

We now have two extreme situations, those for the PH_2 and CO bridges. We understand each well and summarize the pattern of frontier orbitals in **15**. The level filling specified is that of the 42-electron species. We also note here that the observed level patterns fit well with the similar calculations of Mealli.[15a]

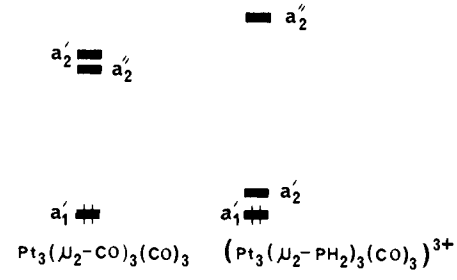

15

What about other bridging ligands, such as μ_2-CNH or μ_2-SO_2? The situation for both of these is closer to μ_2-CO than μ_2-PH_2, as one would expect. But there are some important differences.

Since the a_2'' orbital, the LUMO of $Pt_3(CO)_6$, is composed predominantly of bridging CO π^* (see **10** and **12**), one would expect that changing the bridging ligand would have a significant effect on the redox potential of this type of molecule. This is evidenced by calculations on $Pt_3(\mu_2\text{-}CNH)_3(CNH)_3$ (**8b**) in which the ordering of the unoccupied frontier orbitals differs from that of the CO complex **8a**. The HOMO in both of these 42 valence electron species (a_1') being mostly metal remains at about −12 eV. For the CNH complex the LUMO is of a_2' symmetry, equivalent to **11**, the in-plane CO π^*, Pt combination. At 0.4 eV higher energy the out-of-plane a_2'' orbital equivalent to **10** appears. There are a number of factors at work here to cause this sequence reversal. First the CNH π^* orbitals are around 1 eV higher in energy than the CO orbitals leading to less interaction with the appropriate metal orbitals (according to the energy difference term in the denominator of the usual perturbation energy expression). This effect is realized in a larger HOMO–LUMO gap for the CNH compound **8b**. The positions of the frontier orbitals of all the complexes calculated are indicated in Figure 6. Second, since the a_2'' orbital is metal–bridging ligand π in character whereas the a_2' orbital is σ, the former is affected to a greater extent by changing the ligand. This second point can be appreciated more readily by comparing **10** and **11**.

For compounds such as those with bridging SO_2 ligands life is a little simpler. Unlike CO or CNH, SO_2 has only one low-lying acceptor orbital of π symmetry. The perpendicular sulfur p orbital (in the plane of the SO_2 triangle) is much higher in energy and is involved in S–O antibonding (σ^*). Whereas in **12** there are two sets of CO π-type orbitals (perpendicular a + e sets), $(SO_2)_3$ has one set. The structure of compounds containing a (μ_2-SO_2) ligand indicates that the coordination about S is quasitetrahedral. As a result, the orbitals of the $(SO_2)_3$ fragment resemble the a_2' + e′ combination shown for $(CO)_3$ in **12**.

This time the a_2'' orbital of the $Pt_3(CO)_3$ fragment (Figure 1) remains localized on the terminal CO's and is not stabilized to any great extent. The a_2' orbital on the other hand interacts with its symmetry counterpart on the $(SO_2)_3$ fragment leading to a low-lying bridging SO_2–Pt combination. Figure 6 summarizes these results; for the neutral complex $Pt_3(\mu_2\text{-}SO_2)_3(CO)_3$ (**8c**) the a_2' orbital is the LUMO. The above analysis is in keeping with the results of similar calculations on this compound by Mingos and co-workers.[15b] The calculations also suggest that favorable HOMO–LUMO gaps will result for both the 42 and 44 valence electron species (the a_2' orbital is the LUMO or HUMO, respectively). This then brings us to the reduced triangular clusters.

The Monomer with 44 Electrons

First let us consider the $\{Pt_3(CO)_3[Fe(CO)_4]_3\}^q$ clusters **4**, where q = 1− or 2−. The bonding in this structure, with particular emphasis on the bridging $Fe(CO)_4$ (C_{4v}) groups, has been discussed previously.[14g,15a] Before proceeding in our discussion, we must make explicit the formalities of our electron counting scheme and how it differs from that used previously.

When q = 2−, the polyhedral skeletal electron pair approach,[17] which counts the valence electrons of each $Fe(CO)_4$ group, reaches an electron count of 86. In this formalism each CO ligand is considered as being a two-electron σ donor and all metals (Pt and Fe) being neutral provide all of their electrons to the cluster. Our perspective, however, was to consider the metal–metal bonded Pt_3 triangle as the basic structural unit, tied together electronically and geometrically with a variety of ligands. In this countext, each $Fe(CO)_4$ group becomes no more than another bridging "ligand". We can do this because the frontier orbitals of each of the three $Fe(CO)_4$ fragments[18] combine into a + e sets under D_{3h} symmetry. These orbitals are similar in energy and spacial extent to those of $(CH_2)_3$ (D_{3h}) or $(CO)_3$ (D_{3h})[19] but especially $(SO_2)_3$ (D_{3h}). A difference of course will be that the a_1' + e′ and a_2' + e′ sets will be in the reverse order for $Fe(CO)_4$ but nonetheless the isolobal relationship will hold.

With use of the $Fe(CO)_4$ group as an analogue of CO or SO_2 the electron count of **4** then conforms to the scheme exhibited by the Pt_3L_6 complexes. To be more explicit, when q = 0 there are 42 valence electrons (as yet unprepared) and when q = 2− there are 44 electrons. Oxidation to the 43-electron cluster results in a significant shortening of the Pt–Pt distances (from 2.75 to 2.66 Å).[8b] Longoni and Morazzoni have tentatively assigned a_2' symmetry to the SOMO of **4** on the basis of ESR experiments[20] which is in keeping with our conclusions based on SO_2 and calculations performed by Mealli.[15a] Considering the nodal properties of an a_2' orbital it is not surprising that oxidation causes a decrease in Pt–Pt distance.

It was mentioned in the introduction that although the Ni_3 clusters fitted the aggregation pattern set by the $[Pt_3(CO)_6]_n^{2-}$ clusters, the "trimer" $[Ni_{12}(CO)_{21}]^{4-}$ (see **6**, n = 4) has a further two electrons. The central Ni_3 triangle, unlike the two outer triangles, is bridged by $Ni(CO)_2$ groups. In a similar way to bridging SO_2 and $Fe(CO)_4$ this "ligand" provides a_2' + e′ in-plane π-type orbitals and a a_1' + e′ σ-type set. In particular the in-plane π set is of similar energy to that of SO_2, resulting in a stabilzed a_2' orbital. Reduction by two electrons results in this orbital being occupied and a HOMO–LUMO gap similar to that shown in Figure 6 for compound **8c**.

Apart from the skeletal change described above for the $\{Pt_3(CO)_3[Fe(CO)_4]_3\}^q$ complex (which is also evident in the long Pd–Pd distances of the 44 valence electron cluster Pd_3X-

(18) Elian, M.; Hoffmann, R. *Inorg. Chem.* **1975**, *14*, 1058–1076.
(19) A recent paper describes the similarity between (μ_2-CO) and (μ_2-CH_2) groups: Evans, D. G. *J. Chem. Soc., Chem. Commun.* **1983**, 675–677.
(20) Longoni, G.; Morazzoni, F. *J. Chem. Soc., Dalton Trans.* **1981**, 1735–1737.

$(PPh_2)_2(PR_3)_3$[13b]) there is another change in architecture which we must consider. The cluster $Pt_3(\mu_2\text{-}PPh_2)_3Ph(PPh_3)_2$[8a] mentioned previously has 44 valence electrons and shows a distortion of the metal atoms from a regular equilateral to an isosceles triangle. Two Pt–Pt distances are 2.79 Å, slightly longer than the distances found in the 42 valence electron clusters, and the third is 3.63 Å, clearly too long for any significant metal–metal interaction. It appears that reduction by 2 electrons has broken one of the metal–metal bonds.

To analyze this molecule let us review the situation in the symmetrically bridged cluster $Pt_3(CO)_3(\mu_2\text{-}PH_2)_3^+$ (Figure 5). This 44-electron system has three Pt–Pt bonding orbitals of a_1' + e′ symmetry at low energy, then eleven primarily Pt 5d orbitals, then the a_1' + a_2' frontier orbitals which are both filled.

The 44-electron cluster would be expected to have a longer metal–metal separation, because the a_2' orbital, Pt–Pt antibonding, is filled. Our calculations optimize the Pt–Pt distance at ~3.25 Å. We next studied a lowering of symmetry to C_{2v}, as occurs in the observed 44-e⁻ complex. This was accomplished by varying θ, as shown in **16**. The calculation was repeated at several values

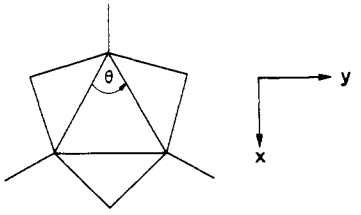

$(Pt_3(\mu_2\text{-}PH_2)_3(CO)_3)^q$

16

of the metal–metal distance. For most distances a rather flat curve with a minimum at 60°, the D_{3h} geometry, results. It takes little energy to open up one bond, and we agree with Mealli[15a] that the reasons for the distortion observed are likely to be steric in origin. An analysis of this deformation has been independently given by Dedieu, Braunstein, and co-workers.[21] For the 42-electron phosphido-bridged system there is an interesting possibility of a double minimum in the potential energy curve, due to a crossing of the orbitals that were a_1' and a_2' in D_{3h} at some θ.

In summary, the bridging ligand has a good deal of influence over the structure and the electron counts of the triangular metal clusters described. For ligands with orthogonal π^* acceptor orbitals such as CO and CNR, stabilization of filled metal orbitals results in a 42-electron species. Ligands with π-donor orbitals such as PR_2^- and the halogens provide counts of 44 electrons by pushing up from the d block an orbital (a_2') which is mainly metal–metal antibonding. Occupation of this orbital then leads to a distortion away from the ideal structure.

The Dimer: $[M_3L_6]_2$

The eagerness of the $Pt_3(\mu_2\text{-}CO)_3(CO)_3$ molecule to form dimers, trimers, etc., of the form $[Pt_2(\mu_2\text{-}CO)_3(CO)_3]_n^{2-}$ is apparent from the literature (see **2a** and **2b**). This propensity for conglomeration is shared to a limited extent by the nickel clusters but not by palladium. It is therefore of interest to determine the electronic reasons for the stacking of monomer units and to understand the differences between the structures of the Pt- and Ni-based oligomers. We begin our study of these higher molecular weight compounds by first asking what happens when two monomer units are brought together in an ideal and highly symmetric way.

Since the Pt chains all carry a 2– charge regardless of the value of n, we considered the construction of the dimer $[Pt_3(CO)_6]_2^{2-}$ from a neutral and a charged monomer under D_{3h} symmetry. Such a fragment orbital interaction diagram in which the distance between monomers (d) is 3.0 Å is shown in Figure 7. As it should

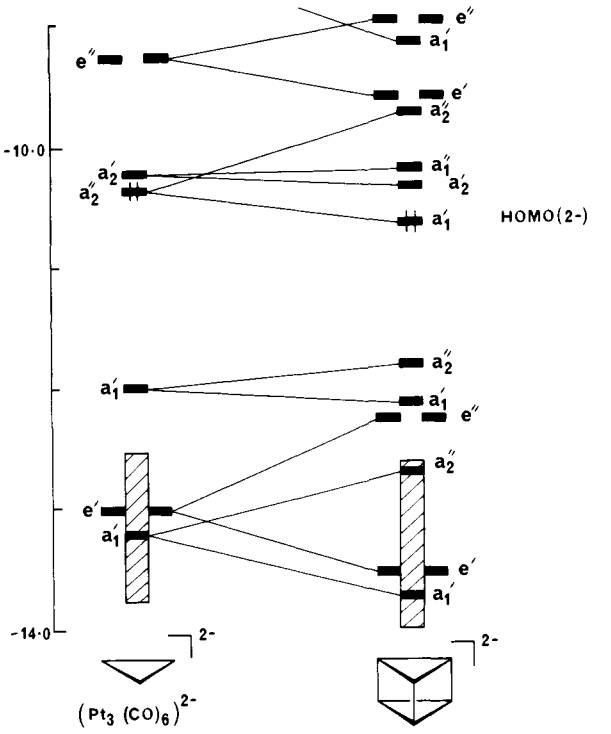

Figure 7. Interaction between two $Pt_3(\mu_2\text{-}CO)_3(CO)_3$ complexes to form $[Pt_3(\mu_2\text{-}CO)_3(CO)_3]_2^{2-}$ maintaining D_{3h} symmetry.

be, those orbitals which are perturbed the greatest are those which lie out of the plane of metals for each monomer (compare Figures 1 and 7).

Since the monomer a_1' and e′ orbitals within the Pt_3 d block (hatched area of Figure 7) are largely d_{z^2} in character, the large overlap resulting from interaction with another monomer under D_{3h} symmetry results in a large energy separation of the in- and out-of-plane symmetry combinations. The next highest a_1' orbital and the a_2' orbital (see **9** and **11**, respectively) are in-plane orbitals and dimerization causes little energy separation in their symmetry combinations.

Importantly, a_2'' of the monomer (see **10**) is clearly directed out of plane and formation of the dimer (d = 3.0 Å) causes the in-phase combination to be about 0.3 eV lower in energy than the monomer a_2''. This orbital becomes the HOMO for the $[Pt_3(CO)_6]_2^{2-}$ species. Further addition of neutral monomer units and growth of the Pt_3 chain will cause the HOMO, always the in-phase combination with a_2'' (monomer) parentage, to decrease in energy. Eventually, as more monomers are added, the discrete molecular orbital picture outlined above will be no longer appropriately descriptive. Instead, bands of orbitals are necessary to detail all phase combinations of each monomer unit in a polymer. We will come to this description a little later.

Recently the $[Pt_3(CO)_6]_n^{2-}$ anions have been studied by X-ray photoemission spectroscopy. In general, the valence spectra for all of the clusters are remarkably similar, especially for the Pt d bands. The major change in the spectra occurs for the CO 5σ and 1π derived bands (involved in metal–CO bonding) which increase in bonding energy as the oligomer size increases (at least until $n \sim 6$[22]). The results of our calculations conform with this observation; the a_1' orbital HOMO of the charged dimer is predominantly CO π^* in character and increasing chain size lowers this orbital in energy.

The question that now arises concerns the balance of energy between filled orbitals which are rising in energy and those which are falling, i.e., is there a minimum in the total energy of the dimer for the "linear" approach of two monomers? Also, is this minimum dependant on the overall charge of the cluster?

(21) Bender, R.; Braunstein, P.; Dedieu, A.; Tiripirchio, A., to be published.

(22) Apai, G.; Lee, S.-T.; Mason, M. G.; Gerenser, L. J.; Gardner, S. A. *J. Am. Chem. Soc.* **1979**, *101*, 6880–6883.

Table I. Summary of Calculations on a Variety of Dimers

compound	symmetry	stabilization energy[a]	OP_{M-M}[b]	d	d_{M-M}*[c]	fragment OP[d]
$[Pt_3(CO)_6]_2^{2-}$	C_2 (slipped)	−0.17				
	D_{3h}	−0.13	0.2065	3.0	3.00	0.2183
	D_{3d}	−0.06	0.2078	3.0	3.37	0.1739
$[Ni_3(CO)_6]_2^{2-}$	D_{3h}	−0.16	0.2034	3.0	3.0	0.1215
	D_{3d}	−0.10	0.2042	3.0	3.30	0.1155
CO's bent back	D_{3d}[e]	−0.56	0.2115	3.0	3.30	0.1644

[a] The energy is relative to the sume of the energies of two monomers (either both neutral or one charged). [b] Overlap population between two metals within a triangle (the Pt–Pt distance is 2.67 Å and the Ni–Ni distance is 2.38 Å). [c] Distance between the closest metals in different triangles. [d] Total overlap population between two monomers. [e] Both terminal and bridging CO's are bent back away from the center of symmetry by 15°.

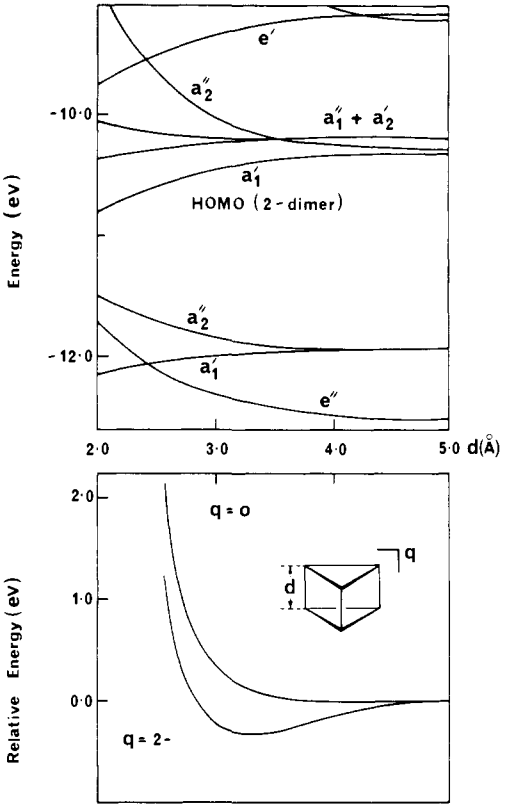

Figure 8. Walsh diagram and relative energy vs. d plot. The linear approach of two monomer units is constrained to D_{3h} symmetry.

Shown in Figure 8 are the relative energy vs. d (the intertriangle separation) curves for the dimer constrained to D_{3h} symmetry. Two curves are shown, one for the neutral dimer and the other for the charged dimer. The energy for the former is relative to two neutral monomers while for the latter it is relative to a neutral and a charged monomer. Also shown in Figure 8 is the associated Walsh diagram for the linear approach.

There is a clear minimum in energy, of about 0.3 eV, at a separation d = 3.3 Å for the charged dimer. The crystallographically observed distance between the Pt_3 triangles is 3.04 Å; the calculations overestimate this separation, but in a qualitative sense they predict a bound state for the charged dimer.[23] The energy curve for the coupling of two neutral monomers emphasizes this conclusion since it is repulsive at all d. We can then consider the extra two electrons as the "glue" holding the triangles together.

The minimum at d = 3.3 Å is also reflected in the Walsh diagram. Most of the energy levels change very little until about d = 3.7 Å, after which they begin to separate into their in- and out-of-phase combinations. The balance in favor of further decreasing d caused by lowering of the energy of the HOMO is altered as the effects of steric repulsion begin to dominate. As a result, soon after $d \sim 3.0$ Å the relative energy curve begins to ascend sharply as filled metal and CO π orbitals rise.

Before moving on to describe the Ni_3 dimers, it is important to present the results for two further distortions of the Pt_3 dimer. The crystal structure of $[Pt_3(CO)_6]_2^{2-}$ (see **1**) indicates that there is a translation or slip of one monomer unit relative to the other. However, calculations suggest that such a distortion, in which d is kept constant at 3.0 Å, produces a structure which is only slightly more stable than the ideal D_{3h} geometry. Presumably, moving away from the eclipsed structure removes some of the filled orbital repulsion. These results are shown in Table I.

Further, higher oligomers (such as the pentamer, **2**) have structures in which some of the monomer units are rotated relative to the others. One can envisage that this is a distortion toward a D_{3d} structure similar to that observed for the Ni_3 oligomers. Indeed ^{195}Pt NMR spectroscopy indicates that there is free rotation of the Pt_3 triangles around the principal C_3 axis and that in solution these triangles are exchanged between chains.[24] Clearly there is not a great deal holding these chains together. Motion about the C_3 axis from D_{3h} to D_{3d} at d = 3.0 Å increases the total energy by only 0.07 eV (see Table I), and the total bonding between the monomers (fragment OP) also decreases. These small energy changes between the trigonal prismatic and trigonal antiprismatic structures are in keeping with the results from the NMR experiments. However, care should be used in interpreting these results since the D_{3d} structure has not been minimized with respect to d, the distance between the monomers.

This brings us to the Ni analogue of the Pt_3 dimer. As mentioned in the introduction, this compound has a trigonal antiprismatic geometry of metal atoms, the antipode of the Pt cluster. It has been suggested that such a difference between a first- and third-row transition element in this cluster type is the result of inherently stronger Pt–Pt bonds at a particular internuclear distance relative to the strength of the Ni–Ni bonds at the same distance. As a result, to achieve the same level of stabilization, the Ni_3 dimer must rotate to the staggered conformation in which each metal has close contacts with two other metals in the other fragment and the steric interactions between the ligands are minimized. However, by comparing the stabilization energies of the D_{3h} and D_{3d} Ni_3 dimers (see Table I), one would predict that at d = 3.0 Å the D_{3h} structure is favored. By relaxing the constraint in which all CO ligands remain in the plane of each Ni_3 triangle, the stabilization energy increases drastically (Table I, CO's bent back). Even though d remains the same a great deal of energy is gained by having the ligands 15° out of the plane (away from the center of symmetry). This geometrical constraint was not relaxed for the Pt dimer, but it is expected that it would have produced similar stabilization.[25] Apart from minimizing the steric interactions between the ligands, bending the CO's back also changes the hybridization at the metal such that the metal-centered orbitals extend further toward the other fragment. On bending the CO's 15° out of the plane, the electron density on

(23) The effects of bending the CO ligands out of the plane of the Pt_3 triangles on d are discussed later for the Ni dimer.

(24) Brown, C.; Heaton, B. T.; Towl, A. D. C.; Chini, P.; Fumagalli, A.; Longoni, G. *J. Organomet. Chem.* **1979**, *181*, 233–254.

(25) Indeed, minimization of the energy with respect to d for the trigonal prismatic Ni dimer led to results similar to those found for the Pt dimer (see Figure 9); viz., the approach was repulsive and for the q = 2− dimer a minimum was found at d = 3.3 Å. This is interpreted as indicating that these minima are caused more by ligand–ligand interaction than by metal–metal interaction.

the metals for the HOMO (a_1') changes from 16 to 25% and mixing of d_{z^2}, p_z, and s gives them more directional character.

As a result of the better overlap, the bonding between the monomers increases. This is reflected in the fragment overlap populations in Table I.

If two $Ni_3(CO)_6$ units are brought together in an octahedral geometry and the ligands allowed to bend out of the Ni_3 plane by 15°, one obtains a repulsive curve for the neutral dimer. For the dianionic species there is a minimum, over 0.7 eV deep, at 2.7 Å. This compares well with the experimentally observed 2.77-Å separation of Ni_3 planes.

In summary, the formation of dimer, trimers, etc., is only favorable for the charged species. The linear approach of two neutral monomers (with the supercluster constrained to either D_{3h} or D_{3d} symmetry) is repulsive. Occupation of the out-of-plane a_1' orbital (derived from the CO π^*, Pt p_z orbital; a_2'' of the monomer) creates a minimum on this path. The depth of this minimum is dependent on whether the CO's are in the plane of the M_3 triangle or are bent out as in the crystallographic structure. The calculations reproduce the separation of monomers more accurately with out-of-plane ligands.

These results have been expressed in a slightly different way by Mingos and co-workers.[15b] Their analysis suggests that for the coupling of two monomer units, stabilization of the HOMO of the charged species is greater for D_{3h} than for D_{3d} symmetry paths (this stems from greater overlap for the a_1' relative to the D_{3d} counterpart, a_{1g}). But countering this effect is the reduction of steric interaction for the staggered D_{3d} geometry. The final balance will depend on these effects and also the differences in bonding propensities between Pt and Ni, i.e., the inherently greater bonding between Pt–Pt compared to Ni–Ni at a particular internuclear separation.

Polymer; $[M_3L_6]_\infty$

One can extend the process of addition of Pt_3 triangles to the dimer to produce trimers, tetramers, pentamers, etc. As the number of units in the oligomer is increased the discrete molecular orbitals merge into bands. By the time ten monomer units have been assembled it is expected that the electronic structure of the oligomer would be better represented by a band structure rather than by a molecular orbital picture. By resorting to band calculations of the hypothetical $^1[Pt_3(CO)_6]^q_\infty$ one-dimensional polymer shown in **17**, one can gain a better insight into the requirements of oligomeric aggregates.

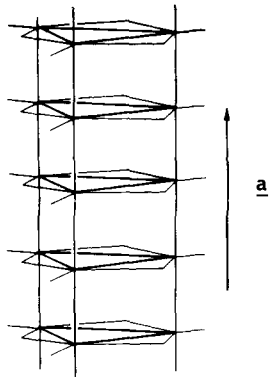

$^1(Pt_3(CO)_6)_\infty$

17

The electronic structure of **17**, shown in Figure 10, was calculated with the tight binding (LCAO) method.[26] Since **17** has a regular structure in the direction *a*, i.e., the distance between the Pt_3 triangles is constant, the unit cell was chosen to contain one monomer unit with D_{3h} site symmetry. The symmetry of the chain at all *k* points is C_{3v} since only the C_3 axis (coincident with *a*) and the vertical mirror planes leave the wave vector unaltered for all *k*. The horizontal mirror planes of D_{3h} carry *k* to $-k$.[27]

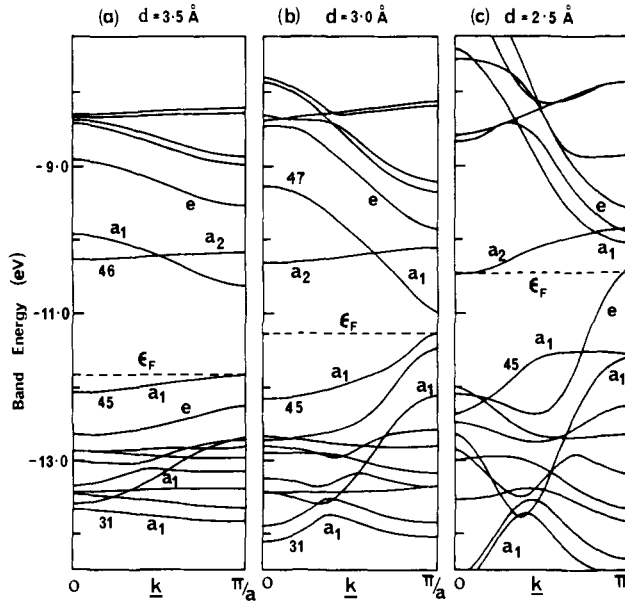

Figure 9. Band structures for the first Brillouin zone of $^1[Pt_3(\mu_2\text{-}CO)_3(CO)_3]_\infty$ for various intertriangular separations: (a) d = 3.5 Å, (b) d = 3.0 Å, (c) d = 2.5 Å

Again the separation between the monomer units is of interest here as with the dimer. Beginning with this structural feature, the band structure was calculated for d = 3.5, 3.0, and 2.5 Å. These are included in Figure 10. Before examining this distortion consider the band structure for d = 3.5 Å (Figure 9).

For the neutral chain $^1[Pt_3(CO)_6]_\infty$, the Fermi energy is −11.8 eV. Band 45 with a_1 symmetry (a_1' site symmetry) is the crystal orbital equivalent of **9** drawn for the monomer. Since this is an in-plane orbital the dispersion across the Brillouin zone is small. Toward the zone edge ($k = \pi/a$), some mixing of d_{z^2} occurs and the band climbs in energy.

The lowest vacant band at k = 0 is of a_2 symmetry and above this is a band of a_1 symmetry. They correspond to **11** (a_2', D_{3h}) and **10** (a_2'', D_{3h}), respectively. The difference here is that their order is reversed (at k = 0) from that in the monomer and the dimer. The reason is clear when one realizes that band 47 is composed of mainly CO π^* out-of-plane mixing with metal p_z. As expected there is a steady decrease in energy of this band as the zone is crossed since the bonding between unit cells becomes greater. This change is due to the difference in the phase factor on translation across the zone (at the zone edge the crystal orbitals are antisymetric with respect to translation by *a*). Band 46 (k = 0) is mainly localized in the Pt_3 triangle plane and is almost dispersionless across the zone.

Applying pressure to the chain in the direction of *a* will decrease the separation between the Pt_3 triangles. When d = 3.0 Å a large reorganization of the band structure has already occurred (Figure 9). Band 47 at k = 0 is now more antibonding and therefore higher in energy while at the zone edge it is more bonding and lower in energy. Band 46 (k = 0) remains almost dispersionless. Below the Fermi energy for the neutral chain (ϵ_F = −11.3 eV) the situation becomes more complex due, in the main, to a number of bands mixing orbital character. Band 31 (k = 0) is mostly d_{z^2} in character and bonding between unit cells. As the degree of phase change between unit cells increases across the zone this band rises in energy and crosses a number of other bands of a_1 symmetry. Eventually, d_{z^2} orbital character appears in band 45 close to $k = \pi/a$ and in band 47 at $k = \pi/a$.

(26) (a) Whangbo, M.-H.; Hoffmann, R. *J. Am. Chem. Soc.* **1978**, *100*, 6093–6098. (b) Whangbo, M.-H.; Hoffmann, R.; Woodward, R. B. *Proc. R. Soc. London, Ser. A* **1979**, *366*, 23–46.

(27) For example, see: Lax, M. "Symmetry Principles in Solid State and Molecular Physics"; John Wiley and Sons: New York, 1974.

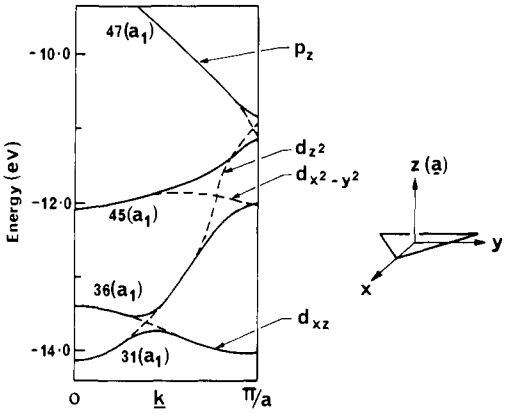

Figure 10. Selected parts of the band structure of $^1[Pt_3(CO)_6]_\infty$ for d = 3.0 Å showing the rise of d_{z^2} crystal orbital character to the band gap.

It is this crossing of the Pt d_{z^2} crystal orbital character into higher bands that causes the decrease in band gap. Figure 10 is a simplified band structure at d = 3.0 Å showing the travels of the d_{z^2} band.

Further decrease in d to 2.5 Å (Figure 9) causes an increase in the energy difference between the a_1 bands at the gap as orbital character is swapped between them. At this distance, however, a band of e symmetry is pushed into the band gap and becomes the highest occupied crystal orbital in parts of the Brillouin zone. This orbital is also mainly d_{z^2} and interacts with a higher lying empty e band of p_z character at $k = \pi/a$. This situation is completely analogous to the changes in the band structure of the tetracyanoplatinate chains as the distance between metals is reduced.[26a] **18** and **19** are the crystal orbitals of p_z (a_1) and d_{z^2} (a_1), respectively, at $k = \pi/a$. The p_z band is antisymmetric with

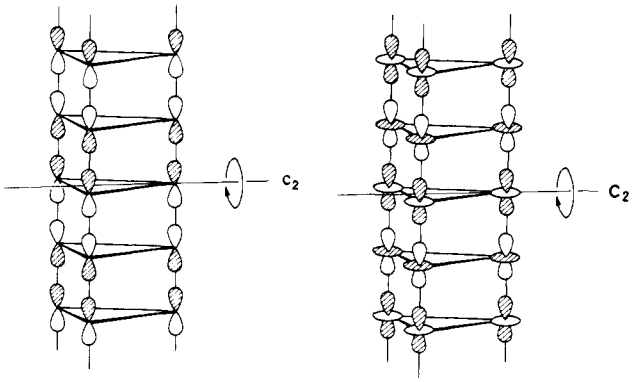

18 **19**

respect to rotation about the C_2 axis while the d_{z^2} band is symmetric. At $k = \pi/a$ these bands are permitted to cross, since they have different symmetry properties.

Figure 11 is a plot of the total energy of the unit cell relative to the total energy of the monomer for both the neutral and charged (1−) polymers. As can be seen from this figure, both electron counts lead to an increase in total energy as the chain is compressed. Surprisingly, the repulsion energy is the same in both chains, with the charged chain showing slightly greater repulsion at smaller d. It is not surprising that there is no minimum located for the compression reaction coordinate. Recall that in Figure 8, the potential surface for the linear approach of two neutral monomers was also repulsive.

For the series $[Pt_3(\mu_2\text{-}CO)_3(CO)_3]_n^{2-}$ the charge remains the same for all oligomers up to n = 10, which is understandable in terms of occupation of the a_1' orbital of the dimer thus providing the "glue" to hold the chain together (see Figure 8). In the n = 10 case, each Pt_3 monomer has a charge of −0.2 (−2/10), and for this electron count the p_z band will be partially occupied. It is

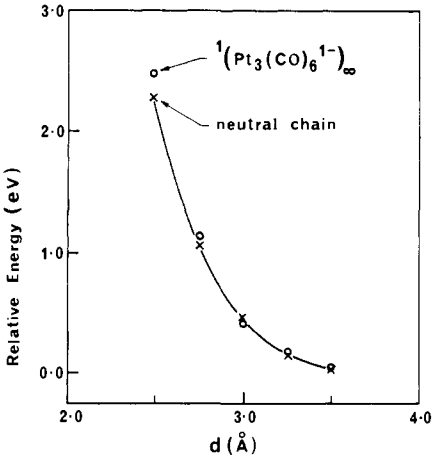

Figure 11. Comparison of the total relative energy per unit cell for $^1[Pt_3(CO)_6]_\infty$ (×) and $^1[Pt_3(CO)_6^{1-}]_\infty$ (○) as the distance d is varied. The energies are relative to $Pt_3(CO)_3$ and $Pt_3(CO)_3^{1-}$, respectively.

the lower part of this band which is bonding between unit cells (see **18**). As more electrons are added to the chain and this band fills, the antibonding between unit cells increases. Clearly from Figure 12 half-filling the p_z band has altered the balance so that decreasing d is met with an energy barrier.

A similar situation was observed in the study of the tetracyanoplatinate chains.[26a] For these compounds, which are similar in many ways to the chain of interest here, partial oxidation led to a minimum in the energy vs. separation plot. Since in $^1[Pt_3(CO)_6]_\infty$ the d_{z^2} orbital also appears at the gap, partial oxidation may effect some overall stabilization of the polymer.[28]

Partially occupied bands, especially those showing large dispersion across the zone, are likely to lead to metallic conductivity unless they can stabilize in some way. Such stabilization occurs with Peierls distortions in which a geometric change breaks the symmetry of the chain and opens a band gap, thereby lowering the total energy. With a band which has only one-tenth (0.2/2.0) of its maximum number of electrons such a distortion may be evident over 10 monomer units and repeatable thereafter. Perhaps the helical-type distortions observed in the crystal structure of the pentamer **2** (and presumably in the decamer) are a result of such electronic demands. However, it should be noted that these distortions are by no means regular and may be due to crystal packing forces.

Intercalates

An interesting class of compounds are those in which an atom is enclosed in the cavity produced by the stacking of metallic ring systems. Carbides or nitrides with C or N trapped in octahedral or trigonal prismatic holes are well known in both molecular and extended systems.[29]

There are two intercalates of the Pt dimers known. The first is $[Pt_3(\mu_2\text{-}CNR)_3(CNR)_3]_2Hg$ (**20**) in which R = 2,6-dimethylphenyl[30] and the second is $[Pt_3(\mu_2\text{-}CO)_3(PPh^iPr_2)_3Hg]_2$ (**21**).[31] There is an important difference, however, between the

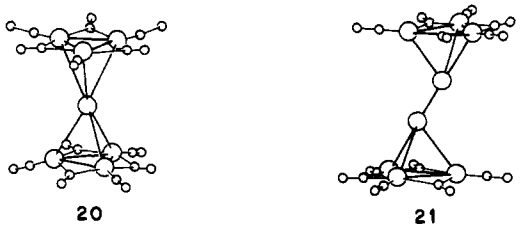

20 **21**

(28) The relative energy vs. d curve for $[Ni_3(CO)_6]_2$ (D_{3d}) with the CO's bent back shows a slight minimum at about d = 2.6 Å for the oxidized dimer, i.e., $[Ni_3(CO)_6]_2^{2+}$. This minimum is only around 0.2 eV deep compared to 0.7 eV for the reduced dimer.

(29) See references in the following: Wijeyesekera, S. D.; Hoffmann, R. *Organometallics* **1984**, *3*, 949–961.

(30) (a) Yamamoto, Y.,; Yamazaki, H.; Sakurai, T. *J. Am. Chem. Soc.* **1982**, *104*, 2329–2330. (b) Yamamoto, A., private communication.

Table II. Stabilization Energy for Capped Pt Monomers

compound	fragment I	fragment II	stabilization energy (eV)
CO model of **20**	$n = 2$	Hg	−7.30
CO model of **21**	$n = 2$	Hg_2	−5.84
$[Pt_3(\mu_2\text{-}CO)_3(CO)_3]Hg$	$n = 1$	Hg	−6.89
$[Pt_3(\mu_2\text{-}CO)_3(CO)_3]Hg_2^{2-}$ [a]	$n = 1$	$(Hg\cdots Hg)^{2+}$ [b]	−12.11
$^1[Pt_3(\mu_2\text{-}CO)_3(CO)_3Hg]_\infty$	atoms within unit cell		−0.63[c]

[a] This compound has both faces of the Pt_3 triangle capped with Hg (closo). [b] The distance between the Hg ions is 5.0 Å. [c] Stabilization energy is relative to $[Pt_3(\mu_2\text{-}CO)_3(CO)_3]Hg$.

nitrides and carbides and the mercury complexes. The former show bonding between all the metal atoms whereas in the latter there is metal–metal bonding only within a triangle. In **20**, the Pt_3 triangles show a distorted trigonal prismatic relationship in which one is rotated by 11° with respect to the other. Again the metal–metal distance within a triangle is of the order of a single bond (2.64 Å), but now there is no significant through space interaction between triangles as evidenced by the distance of 5.0 Å. This complex is held together by Pt–Hg bonds (Pt–Hg 2.94 Å).

With **21**, the two Pt_3 triangles are related by a center of symmetry and are therefore staggered with respect to each other. Again, there is metal–metal bonding within a triangle, but the distance between triangles (~6.0 Å) precludes significant interaction. The Hg–Hg separation is 3.2 Å, slightly longer than is found in the crystalline α form of metallic Hg (2.99 Å) but significantly longer than that found in mercurous halides (2.4–2.7 Å).[32] From these data **21** could then be considered as two Hg-capped Pt_3 triangular clusters joined weakly by Hg···Hg interactions rather than a Pt_3 dimer intercalate. Even so, the capping shows some distortion in that two Hg–Pt distances are slightly longer than the other four (all are in the range 2.9–3.1 Å).

There are a number of ways to count the electrons of clusters **20** and **21**. Beginning with **20** we can consider the mercury as Hg^{2+} having a full d block and no s electrons, thereby requiring the platinum triangles to be $(Pt_3L_6)_2^{2-}$, in correspondence with the dimers discussed previously. Likewise for **21** if we count the dimercury as Hg_2^{2+} demanding a Hg–Hg bond, we also arrive at $(Pt_3L_6)_2^{2-}$. Alternatively, relaxing the requirement of a formal Hg–Hg bond, **21** can be considered as two $(Pt_3L_6)^{2-}Hg^{2+}$ units. Since the cluster is only weakly bound at Hg, the electron-counting formalism is between the $(Hg\text{–}Hg)^{2+}$ and $(Hg\cdots)^{4+}$ extremes.

Another electron-counting scheme begins with neutral Hg. This time complexes **20** and **21** are built from Hg with a filled s orbital and neutral (Pt_3L_6) fragments. From this point of view complex **20** is composed of Hg and two (Pt_3L_6) units and **21** is composed of coupled (Pt_3L_6) Hg units. This approach to counting electrons in these clusters is supported by recent ESCA studies which suggest that for **20** the oxidation state of Hg is close to neutral.[30b] Therefore we will adopt this latter counting scheme in our analysis of these intercalates.

Let us begin with an analysis of the bonding in complex **20**. This is just a simple extension of the bonding in the dimers. As a model of **20** we chose D_{3h}, $[Pt_3(\mu_2\text{-}CO)_3(CO)_3]_2Hg$. Our molecular orbital analysis then simplifies to the interaction of the fragment $[Pt_3(\mu_2\text{-}CO)_3(CO)_3]_2$, d = 5.0 Å, with Hg. This is shown in Figure 12. Since the mercury d block is low in energy and the symmetry disallows hybidization of its orbitals, there is little interaction with the $[Pt_3(CO)_6]_2$ mainly d orbitals. As a result these orbitals are not shown.

The main interaction between the fragments is by way of the Hg 6s and the a_1' orbitals of the metal triangle combination. To a first approximation and according to Figure 12 this involves the interworking of three such orbitals two of which are filled. Combining these orbitals to form the complete complex results

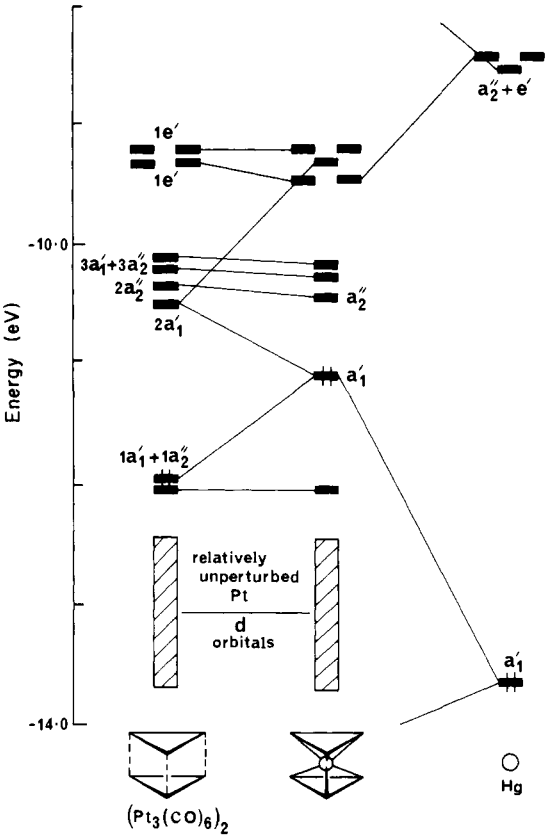

Figure 12. Interaction between $[Pt_3(\mu_2\text{-}CO)_3(CO)_3]_2$, d = 5.0 Å, and the s and p orbitals of Hg. The Hg d block is not shown, it lies about 3 eV lower in energy than the Pt d block.

in three molecular orbitals again with two filled. Simply, if we consider the complex as composed of $[Pt_3(CO)_6]_2$ and Hg (i.e., the Hg 6s orbital is now filled), their combination is initially a repulsive four-electron interaction between $1a_1'$ and Hg 6s. This is then kept favorable by the action of $2a_1'$, which stabilizes the antibonding combination of the HOMO–HOMO interaction. Recall that the $2a_1'$ orbital along with $2a_2''$, $3a_1'$, and $3a_2''$ are predominantly CO π^*. As a result, one would expect that compounds without low-lying orbitals of this type, such as compounds with bridging phosphines, etc., would not favor, energetically, the interaction with Hg. As yet intercalates with other than π^* acceptor bridging and/or terminal ligands have not been prepared.

Table II contains the stabilization energy for the combination of a variety of $[Pt_3(CO)_6]_n$ and Hg_m (m = 1 or 2) fragments. It is clear from this comparison that capping of $Pt_3(CO)_6$ results in a large energy gain. Intercalation of Hg into the dimer, i.e., **20**, is more favorable than incorporation of Hg_2 as in **21**. For this compound, the HOMO is now of a_{2u} symmetry composed of out-of-phase Hg 6s orbitals and the out-of-phase combination of Pt p_z and CO π^* (the a_2'' for the single Pt_3 triangle).

It should be mentioned at this point that calculations have been performed on a model of $\{Ni_3(\mu_2\text{-}CO)_3(CO)_3[M(CO)_5]_2\}^{2-}$ (M = Mo or W) by Mingos and co-workers.[15b] This type of complex can be regarded as a bicapped $Ni_3(CO)_6$ cluster in which the capping groups, $M(CO)_5^{1-}$, are isolobal to H and thus to Hg^+ (see

(31) Albinati, A.; Moor, A.; Pregosin, P. S.; Venanzi, L. M. *J. Am. Chem. Soc.* **1982**, *104*, 7672–7673.
(32) Wells, A. F. "Structural Inorganic Chemistry", 3rd ed.; Oxford University Press: London, 1962.

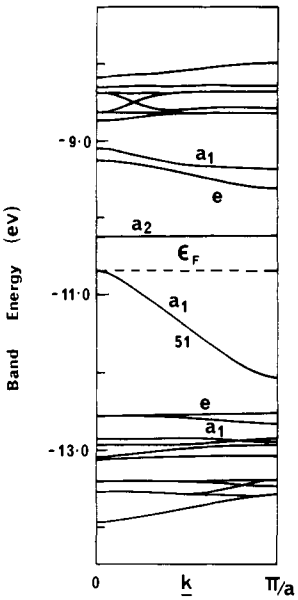

Figure 13. Band structure of $^1[Pt_3(CO)_6Hg]_\infty$.

Table III. Parameters Used in Extended Hückel Calculations

orbital		H_{ii} (eV)	ζ_1	ζ_2	C_1[a]	C_2[a]
H	1s	−13.60	1.300			
C	2s	−21.40	1.625			
	2p	−11.40	1.625			
N	2s	−26.00	1.950			
	2p	−13.40	1.950			
P	3s	−18.60	1.600			
	3p	−14.00	1.600			
O	2s	−32.30	2.275			
	2p	−14.80	2.275			
S	3s	−20.00	1.817			
	3p	−13.30	1.817			
Cl	3s	−30.00	2.033			
	3p	−15.00	2.033			
Ni	4s	−8.84	2.100			
	4p	−4.90	2.100			
	3d	−12.99	5.790	2.000	0.5692	0.6302
Pt	6s	−10.75	2.550			
	6p	−5.27	2.550			
	5d	−13.16	6.010	2.696	0.6332	0.5512
Hg	6s	−13.68	2.649			
	6p	−8.47	2.631			
	5d	−17.50	6.436	3.032	0.6438	0.5215

[a] These are the coefficients in the double-ζ expansion.

entry 4, Table II). In their model the H---H replacement of $(CO)_5M^-$---$M(CO)_5^-$ has orbitals which transform as a_1' and the out-of-phase combination, a_2''. In essence, both a_1' and a_2'' are involved in three-center interactions with a relatively nonbonding a_2'' combination intervening as the HOMO.

Mealli has also studied mono- and bi-capped M_3 triangles, and depending on the type of capping ligand delocalized L–M_3 or localized L–M bonds result.[15a]

An interesting extension to this process of capping is to postulate the existence of a long-chain polymer with the basic structure shown in **22**. We call this the Asao polymer after the researcher who first suggested it.[33] From Table II it is clear that capping of, and intercalation into, these metal triangles proceeds with large energy gains. Even the Ni counterpart to the Pt trimer shows a tendency to have hydrogen reside in the octahedral holes produced by the metal atoms (see **6**). Calculations on $^1[Pt_3(CO)_6Hg]_\infty$ using an idealized geometry based on **20** show that there is increased stabilization gained by polymerizing the monomer $Pt_3(CO)_6Hg$ (see Table II), although this gain is small. The band structure of **22** is shown in Figure 13. Most of the bands are very flat, except for the a_1 band 51, the highest occupied crystal orbital of the neutral polymer. At the zone center, the band is

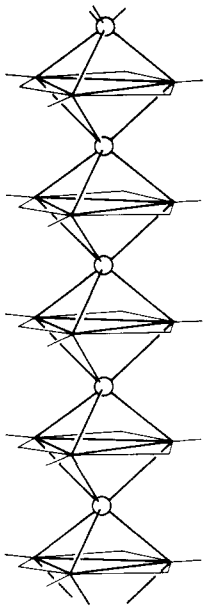

$^1(Pt_3(CO)_6Hg)_\infty$

22

antibonding between unit cells (compare with the HOMO of Figure 12), while at the zone edge it is bonding. Oxidation of **22** will remove electrons from antibonding orbitals, and this should stabilize the chain further as well as producing phenomena related to partially filled bands. If the band is half full, as for $^1[Pt_3(CO)_6M]_\infty$ where M = Cu, Au, or Ag, then typically a pairing distortion will occur such that the unit cell is doubled and a band gap appears at the Fermi energy. Such a distortion will not be expected to produce a large band gap and a semiconductor will result.

Acknowledgment. We are grateful to D. M. P. Mingos and C. Mealli for communication of their work to us prior to publication. Also, we acknowledge a grant from CSIRO to D.J.U. which made his stay at Cornell possible. Part of this work was supported by the National Science Foundation via Research Grant CHE7828048.

Appendix: Computational Details

All calculations that were performed were with the extended Hückel method[34] with weighted H_{ij}'s.[35] The parameters used in these calculations are listed in Table III. Main-group parameters are taken from previous publications.[14f,18] Ni parameters were also taken from previous publications,[36] and the Pt H_{ii}'s were determined by a charge-interative procedure using standard exponents. Hg 6s and 6p parameters were taken from a charge iteration on $Mo(CO)_5Cl(HgCl)$, with *A*, *B*, and *C* parameters for Hg taken the same as those of Cd.

Calculations performed on model compounds were done so with geometries based on known complexes. Bond distances used throughout include Pt–Pt = 2.67 Å, Ni–Ni = 2.38 Å, C–O(terminal) = 1.16 Å, C–O(bridging) = 1.20 Å, Pt–H = 1.70 Å, S–O = 1.45 Å, P–H = 1.44 Å.

Registry No. 2a, 97973-49-4; **8b**, 97919-63-6; **8c**, 97950-28-2; **8d**, 97919-62-5; $[Pt_3(\mu_2\text{-}CO)_3(CO)_3]$, 97919-61-4.

(33) Nakamura, A., private communication, Osaka, 1983.

(34) Hoffmann, R.; Lipscomb, W. N. *J. Chem. Phys.* **1962**, *36*, 2179–2189; **1962**, *37*, 2872–2883. Hoffmann, R. *Ibid.* **1963**, *39*, 1397–1412.
(35) Ammeter, J. H.; Bürgi, H. B.; Thibeault, J. C.; Hoffmann, R. *J. Am. Chem. Soc.* **1978**, *100*, 3686–3692.
(36) Hoffman, D. M.; Hoffmann, R.; Fisel, C. R. *J. Am. Chem. Soc.* **1982**, *104*, 3858–3875.